Histol Histopathol (2024) 39: 1643-1658

Histology and Histopathology
From Cell Biology to Tissue Engineering

ORIGINAL ARTICLE Open Access

Protection of Qingfei Xieding prescription from idiopathic pulmonary fibrosis by regulating renin-angiotensin and ferroptosis in MLE-12 cells

Lifang Sun[1,2], Xinxin He[3], Jiao Kong[4] and Jianying Zhou[1]

[1]Department of Respiratory and Critical Care Medicine, The First Affiliated Hospital, Zhejiang University School of Medicine, [2]Department of Tuberculosis, Hangzhou Red Cross Hospital, [3]School of Clinical Medicine, Hangzhou Medical College and [4]The Second Clinical Medical College, Zhejiang Chinese Medical University, Hangzhou, PR China

Summary. Idiopathic pulmonary fibrosis (IPF) is a lifelong lung disease, but there is no specific drug for treatment. Qingfei Xieding prescription (QF) is active in the treatment of lung diseases. More comprehensive mechanisms over how QF exhibits anti-pulmonary fibrosis need to be elucidated. TGF-β was used to construct a pulmonary fibrosis cell model *in vitro*. Bleomycin was applied to induce a lung tissue fibrosis model in mice *in vivo*. Flow cytometry was used to detect cellular ROS and lipid oxidation levels. Cell substructure was observed by Transmission Electron Microscopy. ELISA was used to determine the levels of inflammatory factors. HE staining, Masson staining and immunohistochemistry were performed to evaluate the degree of fibrosis. Western Blot assay was used to determine the protein expressions of different molecules. In TGF-β-exposed lung epithelial MLE-12 cell model, α-SMA and Collagen I were significantly elevated and cell viability was reduced. QF treatment restored the cell viability decreased by exogenous TGF-β. Ferroptosis inducer Erastin administration could reverse the beneficial effects such as lipid oxidation and ROS reduction caused by QF treatment. QF was proven to inhibit ferroptosis and alleviated the process of IPF by activating ACE2 signal axis. In bleomycin induced IPF mice model, QF altered lung coefficient, body weight and the expression of inflammatory factors, which were prevented by ferroptosis activator Erastin. QF was demonstrated to affect the ACE2-ERK signaling axis *in vivo*. QF alleviated idiopathic pulmonary fibrosis by regulating renin-angiotensin through blocking ferroptosis. This research offers evidence for the potentiality of QF in clinical application for IPF therapy.

Key words: Idiopathic pulmonary fibrosis, Qingfei Xieding prescription, Ferroptosis, ACE2

Corresponding Author: Jianying Zhou, Department of Respiratory and Critical Care Medicine, The First Affiliated Hospital, Zhejiang University School of Medicine, Hangzhou 310003, PR China. e-mail: zjyhz@zju.edu.cn

www.hh.um.es. DOI: 10.14670/HH-18-746

Introduction

Idiopathic Pulmonary fibrosis (IPF) is caused by various injuries to the lungs, including toxic, autoimmune, drug-induced, infectious or traumatic injury (Ley and Collard, 2013). The median survival from diagnosis is 3 to 5 years and the prognosis and clinical course of pulmonary fibrosis are relatively unpredictable because the natural history of the disease varies widely between patients (Harari et al., 2017; Meyer, 2017; Strongman et al., 2018). At present, immunosuppressive agents combined with glucocorticoids, lung transplantation and other methods are mainly used in clinical practice. Treatment, or the use of pirfenidone, nintedanib and other drugs are used to delay its progression, but no specific drugs with good efficacy and few adverse reactions have been found (Fraser and Hoyles, 2016; George et al., 2016). Thus, new understanding of the mechanisms of pulmonary fibrosis and novel treatment methods are urgently needed.

Angiotensin system antagonists block experimental pulmonary fibrosis in various animal models. Numerous *in vivo* studies have shown that Angiotensin II (ANGII) plays a very important role in IPF by blocking ANGII synthesis or its function (Uhal et al., 2012). The application of angiotensin converting enzyme (ACE) inhibitors to inhibit the production of ANGII has been shown to alleviate experimental IPF in animal models induced by various drugs (Wang et al., 2000; Molteni et al., 2007). ACE2 is considered a promising therapeutic target for pulmonary hypertension such as pulmonary hypertension, pulmonary fibrosis and other processes

(Shenoy et al., 2011). It is reported that ACE2 activators attenuate bleomycin-induced IPF progression in a mouse model of physical exercise (Prata et al., 2017). Besides, ACE-2 overexpression in the lung or systemically delivering purified ACE-2 alleviate bleomycin-induced pulmonary fibrosis in rats and mice (Uhal et al., 2007; Shenoy et al., 2010). These This evidence demonstrates that ACE2 is an important regulatory target in IPF and ACE2 activation can alleviate fibrosis.

Ferroptosis is a newly discovered iron-dependent programmed cell death with complex regulatory mechanisms involving multiple metabolic networks and signaling pathways (Dixon et al., 2012). Ferroptosis is a potential therapeutic target for various lung diseases, such as acute lung injury, chronic obstructive pulmonary disease, pulmonary fibrosis, lung infections and asthma (Xu et al., 2021). Ferroptosis is associated with paraquat-induced IPF, and the use of ferroptosis inhibitors may be an effective therapy to reduce paraquat poisoning (Rashidipour et al., 2020). The ferroptosis inducer erastin accelerates fibroblast-to-myofibroblast differentiation by promoting lipid peroxidation and inhibiting GPX4 expression, while ferrostatin-1 can inhibit PF and ferroptosis by reducing lipid peroxidation and enhancing GPX4 expression (Gong et al., 2019). Ang II administration can induce inflammation and ferroptosis in astrocytes with the elevation of AT1R, IL-6, IL-1β, COX-2, and GFAP and reduction of GPX4, NRF2 (Li et al., 2021). However, it has not been reported whether ACE2 is related to the ferroptosis pathway in the formation of pulmonary fibrosis.

Due to the wide range of targets, some Chinese Traditional Medicines (CTM) have been shown to have advantages in the treatment of pulmonary fibrosis. For example, the traditional Chinese Medicine Shenkes treats bleomycin-induced pulmonary fibrosis by regulating TGF-β/Smad3 signaling pathway and oxidative stress (Chu et al., 2017). Active components of single herbal and CTM formulations, especially flavonoids, glycosides, and alkaloids, have potential benefits in IPF, the mechanisms of which appear to involve regulation of inflammation, oxidative stress, and gonadotropins, fibrosis signaling pathway (Li and Kan, 2017). Qingfei Xieding prescription (QF) is a new type of CTM. It is a concentrated granule refined from Chinese herbal medicines such as ephedra, almond, gypsum, pueraria, skullcap, silkworm, and Houttuynia cordata (Yuan et al., 2010; Kumar et al., 2014). QF is reported to reduce the degree of proliferation of fibroblasts and the consequent collagen content and improve the development of pathological fibrosis in the lung (Sun et al., 2018). However, mechanistic studies describing the anti-fibrotic mechanism behind QF in the treatment of pulmonary fibrosis are still scarce.

The aim of the study is to explore the effect of QF on renin-angiotensin system and ferroptosis in improving IPF based on *in vitro* and *in vivo* fibrosis models. This research further helps comprehension over the role of QF in the development of pulmonary fibrosis, and provides evidence for treatment prospects of Chinese Traditional Medicine in IPF.

Materials and methods

Qingfei Xieding Prescription Preparation

Qingfei Xieding prescription was gradually refined and produced by Hangzhou Red Cross Hospital. The raw material includes white mulberry root-bark (12 g), rhizoma anemarrhenae (12 g), herba ephedrae (5 g), bombyx batryticatus (8g), semen armeniacae amarum (8 g), gypsum (42 g), houttuynia cordata thumb (15 g), radix puerariae (12 g) and scutellaria baicalensis (10 g) (Fig. 1A). The herbal admixture was soaked in 500 mL pure water for 30 min. The mixture was boiled until 300 mL liquid left, and the extract liquid was collected by gauze filtration as the first part. Another 300 mL pure water was added to the dregs, and boil slowly until 200 mL liquid left. The filtrate was collected as the second part. The two batches of decoction were mixed together and centrifuged at 8,000 rpm for 15 min in cooling mode. The supernatant was transfered, then filtered by vacuum filtration device with 0.22 μm polypropylene microporous membrane (Fig. 1B), and finally stored in ultra-low temperature refrigerator for further experiments.

Drug-containing serum obtained

10-week SD rats (male) were available from Zhejiang Center of Laboratory Animals (ZJCLA). The animal use has been approved by the Institutional Animal Care and Use Committee of ZJCLA (No. ZJCLA-IACUC-20050061). The SD rats were divided into two groups, and were respectively treated with normal saline or QF by intragastric administration twice a day (10 mL/kg for each intragastric administration). On the third day, serum was collected after gavage treatment. Serum was centrifuged at 3000 g for 10 min, inactivated at 56°C for 30 min, and then stored in aliquots at -20°C.

UPLC-Q-TOF-MS

UPLC-Q-TOF-MS was applied to analyze the chemical components of QF. The electrospray ionization (ESI) was served as the ionization source by Q-TOF SYNAPT G2-Si High Definition Mass Spectrometer (Waters, UK). A Waters ACQUITY UPLC Cortecs T3 Column (2.1×100 mm, 1.6 μm) with Cortecs T3 Van Guard (2.1×50 mm, 1.6 μm) was used to make the separation. 2 μL sample was injected into the column for a gradient elution. The column and autosampler temperature were maintained at 35°C and 25°C. The gradient elution was composed of A (acetonitrile) and B (0.1% formic acid in water). The flow rate was set as 0.3 mL/min. The gradient program followed the process below: 0-2 min, 5% A; 2-32 min, 5-100% A; 32-33 min,

100% A; 33-33.5 min, 100-5% A; 33.5-35 min, 5% A.

Cell Culture and treatment

MLE-12 cell mouse lung epithelial cell was purchased from Shanghai Jinyuan Biotechnology Co., Ltd. (Procell, China, SC004), and cultured in Dulbecco's Modified Eagle Medium (Gibco, USA, 11965092) with 5% FBS (Gibco, USA, 10099141) and 1% penicillin and streptomycin (Gibco, USA, 15070063) under 37°C, 5% CO_2 culture conditions. Cells were exposed to recombinant TGF-β (R&D Systems, Inc., USA, P01137) at a concentration of 1 ng/ml for 48 hours. For QF treatment, mice serum containing QF was obtained and administrated to cells.

Western blotting

Total protein of cells ($5x10^6$/well) in 6-well plates and lung tissues were extracted using RIPA lysis buffer (Chu et al. 2017). Protein concentrations were determined with a Bicinchoninic Acid Assay Kit (Beyotime, China, P0010). The supernatants were collected and loaded into SDS-PAGE following by a transmembrane PVDF (Bio-Rad, USA, no. 162-0177). The membranes were blocked in Tris-buffered saline and Tween 20 (TBST, pH 7.6) containing 5% non-fat milk powder at room temperature for 1.5h, subsequently incubated with primary antibodies. Antibodies used were as follows: α-SMA (1:1000, Affnity, AF1032), Collagen I (1:2000, Abcam, ab270993), ACE2 (1:2000, Abcam, ab108252), ERK (1:1000, Abcam, ab32537), p-ERK (1:1000, Abcam, ab184699), COX-2 (1:2000, Abcam, ab179800), ACSL4 (1:1000, Affnity, DF12141), PTGS2 (1:1000, Abcam, ab283574), NOX1 (1:1000, Abcam, ab131088), FTH1 (1:1000, Affnity, DF6278), Gpx4 (1:2000, Abcam, ab125066), GAPDH (1:2500, Abcam, ab9458) at 4°C overnight. The membranes were washed three times with TBST, subsequently incubated with secondary goat anti-rabbit (1:5000, Dianova, Hamburg, Germany) and conjugated to HRP for 1h at room temperature. Then, the bands were covered with an ECL

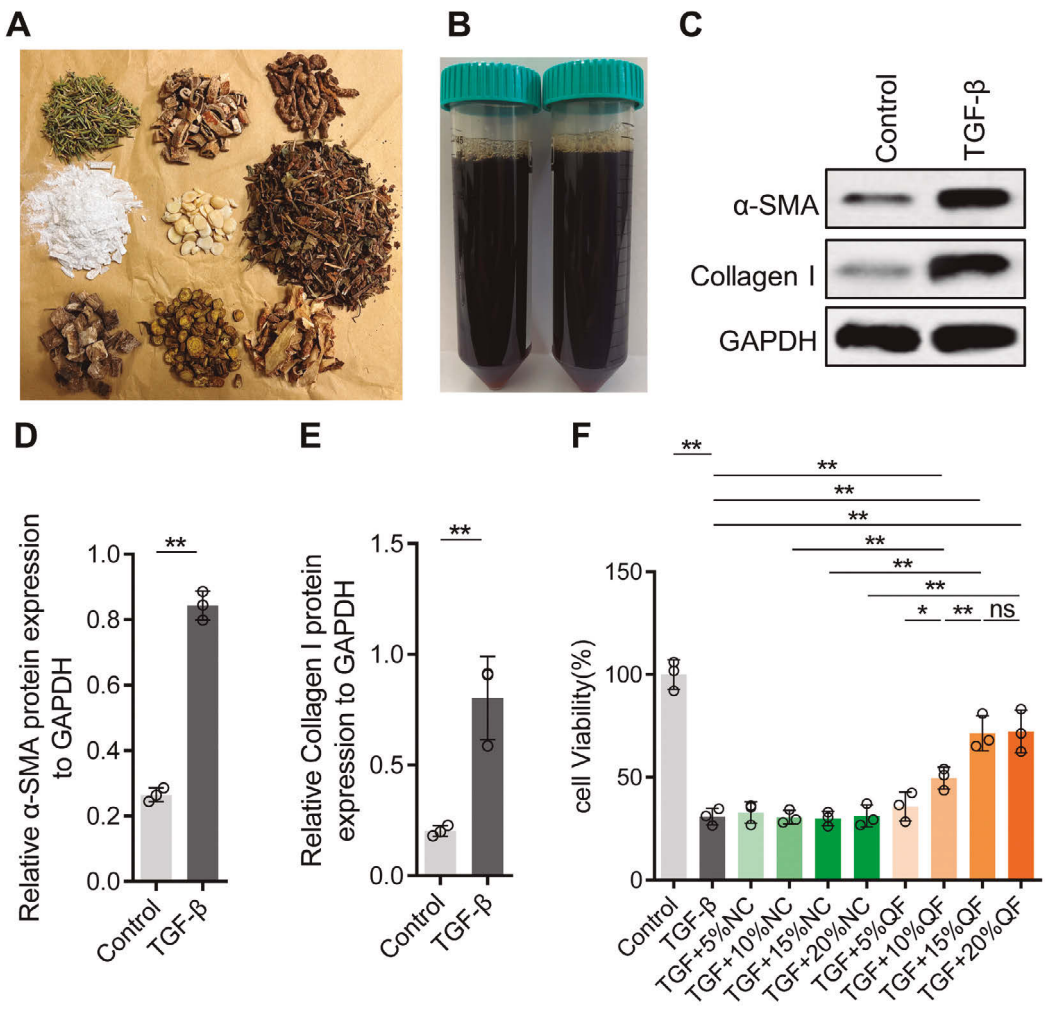

Fig. 1. QF-containing serum inhibited TGF-β-induced fibrosis in MLE-12 cells. **A.** The Chinese herb of QF. The first line (left to right): herba ephedrae (5 g), white mulberry root-bark (12 g), bombyx batryticatus (8 g); The second line (left to right): gypsum (42 g), semen armeniacae amarum (8 g), houttuynia cordata thumb (15 g); The third line (left to right): radix puerariae (12 g), scutellaria baicalensis (10 g), rhizoma anemarrhenae (12 g). **B.** The appearance of the finished QF after 0.22 μm filtration. **C-E.** The expression level of α-SMA and Collagen I were detected by Western Blot. Gray scale analysis was showned in the right panel. **F.** Viability of MLE-12 cells was determined by CCK8 assay in each treatment group. The data in two groups was analyzed with T test. *p<0.05 and **p<0.01.

detection kit (Bio-Rad, USA, no. 170-5060) and visualized using FluorChem E System (Cell Biosciences, California, USA). Band intensities were quantified by ImageJ software (National Institutes of Health, USA).

CCK8 assay

After the cells ($1x10^5$/well) were seeded in 96-well plates and treated with serum containing TGF-β and QF in the following concentration gradient: 5%, 10%, 15% and 20%, MLE-12 cell growth activity was detected by CCK8 kit (Beyotime, China, C0038). Briefly, 100 μL of CCK8 solution was added to each well, and incubated at 37°C in a 5% CO_2 incubator for 2h. Then, the absorbance of each sample at 450 nm wavelength was detected using a microplate reader (Thermo Fisher, USA, Multiskan MK3). Cell viability was calculated using the following formula: experiment group/control group % (Chu et al., 2017).

Immunofluorescence detection of Fe^{2+}

After the cells were cultured on the slides for 24 hours, cells were fixed with 4% paraformaldehyde at 4°C for 15 min and blocked with 5% BSA for 30 min (Li et al., 2021). Subsequently, FeRhoNoxTM-1 was added with Fluorescent probe (Goryo, Japan, GC901) (using a concentration of 5 μM) and incubated at 37°C for 30 min. Cell nucleus was stained with DAPI. And the slides were observed using a fluorescence microscope (Olympus, IX71).

ROS detection (cell and tissue)

ROS level was analyzed using 2,7-dichlorofuorescin diacetate (DCFH-DA) probe according to the description of ROS detection kit (Solarbio, China, D6470) (Li et al., 2021). For MLE-12 cells, after being cultured with serum of QF treatment or control serum, cells were incubated with 10 μM DCFH-DA for 30 min at 28°C. Finally, the cells were analyzed by Flow cytometer (Beckmancoulter, USA, cytoFLEX). For lung tissues, tissues were cut into slices and digested with trypsin, cells for detection were extracted with filter, and then cells for detection were stained using the same procedure as before.

Flow Cytometry (Lipid oxidation detection)

After cells were treated with indicated conditions, cells were digested with 0.25% trypsin without EDTA and collected. The diluted BODIPYTM 581/591 C11 lipid Plasma oxidation probe (Invitrogen, USA, D3861) or CM-H2DCFDA fluorescent probe (Solarbio, China, D6470) was added to the cells and cells were incubated at 37°C for 20 min (Li and Kan, 2017). After cells were washed with serum-free medium 3 times and resuspended in 500 μL PBS, flow cytometer (Beckmancoulter, USA, cytoFLEX) was used to detect the level of lipid oxidation and ROS in cells.

Transmission Electron Microscope

The resulting cells were harvested and fixed with glutaraldehyde in 0.1 M PBS at 4°C for 3-4 hours. The cell samples were washed with PBS and then postfixed with 1% osmium tetraoxide at 4°C. After treatment with 1% uranyl acetate at 4°C for 1h, the cell samples were dehydrated in graded dimethyl ketone and embedded in Epon. A rotating microtome blade was used to cut 60-80 nm-thin sections mounted onto the copper grids. Section and counter staining were conducted with uranyl acetate and Reynold's lead citrate, respectively. The sections were analyzed on a transmission electron microscope (FEI Tecnai G20 TWIN, FEI, USA).

ELISA assay

Serum of each mouse was collected for detection. Levels of IL-6, IL-17 and TGF-β were determined with kits respectively (IL-6, Beyotime, PI326; IL-17, Neobioscience, EMC007; TGF-β, Neobioscience, EMC107b). All procedures were conducted according to the protocol provided. Finally, the optical density (OD value) of each well was measured with a microplate reader at 450 nm wavelength. Using the standard solution and OD value, the best fitting curve equation was drawn, and the corresponding concentration of the sample was calculated by the OD value.

Determination of malondialdehyde (MDA)

The concentrations of malondialdehyde (MDA) in tissue lysates and MLE-12 cells were determined by the MDA assay kit (Beyotime, S0131S) and iron assay kit (Jiancheng, Nanjing, China, A039-2-1), following the respective manufacturer's protocols.

Animal model

All animal experiments were obtained and approved by Zhejiang Center of Laboratory Animals (Animal ethics No. ZJCLA-IACUC-20050061). C57BL/6 male mice were reared for about 8-10 weeks, and the IPF modeling experiment was performed. Mice were treated with bleomycin (dose of 5 mg/kg; Solarbio, IB0871) intravenously for 7 days consecutive injection to induce the IPF model (Chu et al., 2017). Then mice were divided into four groups: Control, IPF mice (IPF), QF therapy IPF mice (IPF+QF), QF therapy and Erastin treatment IPF mice (IPF+QF+Erastin). QF was administered by gavage twice a day for 4 weeks (12 mL/kg per gavage). Erastin was administered intraperitoneally at 30 mg/kg/day for three consecutive weeks (7 days a week). The same volume saline was given to mice in control. Lastly, mice lungs were removed and lung surfaces were flushed with saline and recorded as wet lung weight, while on the other hand,

lung dry weight was determined after incubating samples at 100°C for 48 hours. From the start of drug treatment to one month after the end of treatment (4 weeks and additional 4 weeks, a total of 8 weeks), the survival time of mice was observed, and the death and survival of mice were counted.

HE staining

Mouse lung tissues were obtained and cut into slices. After dehydration, xylene clarification, paraffin immersion and embedding, the tissue was sectioned by a microtome (Leica RM 2016 rotary microtome, Germany); then, the paraffin sections were dewaxed to water. After staining with Mayer's hematoxylin for 5 min, slices were washed with tap water, dipped. Then sections were stained with 1% water-soluble eosin for 5 min, sections were washed at the regular procedures. Finally, after air-drying, the slides were sealed with neutral gum, and the final microscopic examination was carried out (Chu et al., 2017).

Masson staining

After stained with Weigert iron hematoxylin for 5-7 minutes, the slices were rinsed with running water for several minutes. Then 1% hydrochloric acid alcohol was used for differentiation for several seconds, ponceau red acid-fuchsin was used to stain the slices for 3-4 minutes. Next, 1% phosphorus Molybdic acid solution was differentiated for about 5 minutes, dried, and directly counterstained with aniline blue staining solution for 5 minutes without washing with water. Finally, the sections were rinsed with 1% glacial acetic acid for 1 minute (Zhang et al., 2022). The following procedures were the same as HE staining.

Immunohistochemistry

The lung tissue samples were dehydrated and paraffined following routine procedures. Paraffin sections were rinsed in ddH_2O for 3-5 minutes and were blocked with 3% peroxide to ablate endogenous peroxidase. Slices were incubated with anti-Collagen I antibody (1:100, abcam, ab270993) overnight at 4°C. Subsequently, slices were washed four times with PBS and maintained with the secondary antibody for 20 mins at room temperature in the dark. Finally, after slices were dried, images were screened with a microscope (Chu et al., 2017).

Statistical Analysis

GraphPad Prism 6.0 software was used for statistical analysis. For the spectrofotometric measurement results, the curve was made with the standard product. The units of spectrofotometric measurement results were visualized and indicated in graphs according to the formula of the corresponding Kits. Significance for two group was determined with student's two-tailed unpaired t-test. Multiple groups analysis was performed using one-way ANOVA followed by Tukey's post hoc tests. A p value less than 0.05 is considered as statistically significant.

Results

QF treatment attenuates cell viability of MLE-12 cells under the stimulation of exogenous TGF-β

Firstly, the contents of QF were verified by mass spectrometric analysis (Figs. 2, 3, Tables 1, 2). Additionally, the contents of ingredients in the drug-containing serum after taking the QF were also verified. We found that the molecular formulas C24H24O11, C21H20O10 and C20H32O6 were metabolized from the contents of QF which were not observed in control serum (Figs. 4-6). In order to study the effect of QF in the process of IPF, MLE-12 cells were treated with TGF-β (1 ng/mL) to construct a pulmonary epithelial fine fibrosis model *in vitro*, and then western blot assay was conducted to determine the levels of α-SMA and Collagen I, which were the indicators of fibrosis. It was shown that the expression levels of α-SMA and Collagen I in the TGF-β-induced group were significantly increased compared with the control group (Fig. 1C-E). Subsequently, QF-containing serum from SD rats was collected after three days of gavage. Control serum and QF-containing serum were obtained to challenge MLE-12 cells to examine the effect of QF on pulmonary fibrosis. The results of CCK8 assay indicated that cell viability of MLE-12 cells in the TGF-β treatment group was significantly reduced compared to the control group, whereas cell viability was significantly increased when administrated with different concentrations of QF (Fig. 1F). Therefore, QF-containing serum could reverse process of pulmonary fibrosis by attenuating cell viability in TGF-β-exposed MLE-12 cells.

Ferroptosis inducer obstructs the protective effect of QF on TGF-β-induced fibrosis in MLE-12 cells

During the pathogenesis and development of IPF, the cellular level mainly involves cellular biological processes such as inflammation, oxidative damage and the accumulation of ROS (Bringardner et al., 2008). Actually, the ferroptosis process is iron-dependent cell death caused by accumulation of lipid peroxidation, characterized by abnormal accumulation of ROS and decreased glutathione content (Li et al., 2020). Thus, we explored the role of the ferroptosis process during QF-treated pulmonary fibrosis in MLE-12 cells. Firstly, CCK8 assay showed that cell viability of MLE-12 cells was significantly reduced after TGF-β treatment, which was restored with QF-containing serum administration. However, after intervention with ferroptosis inducer Erastin, the cell viability was significantly down-

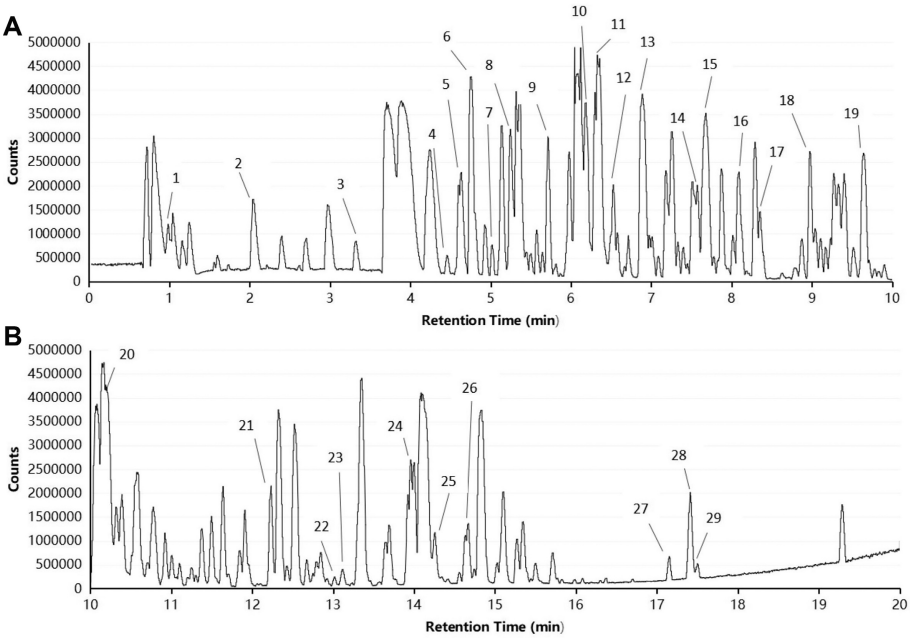

Fig. 2. BPI of extract under the positive ion mode. BPI of extract under the positive ion mode for 0-20 min. **A.** 0-10 min. **B.** 10-20 min.

Table 1. Identification of chemical constituents from extract (screening in the positive ion mode).

No	Observation retention time (tR) (min)	Identification	Element composition	Observed molecular mass (Da)	Molecular mass (Da)	Error (ppm)	Adduct	Fragment ions
1	0.99	Mimosine	C8H10N2O4	198.064	198.06406	-0.3	+H	110.0602; 85.0282; 108.0444
2	2.03	Cinnamic acid	C9H8O2	148.0524	148.05243	-0.1	+H	103.0542; 131.0491
3	3.36	Ephedrine	C10H15NO	165.1151	165.11536	-1.5	+H	148.1121; 133.0886; 150.0913
4	4.49	Isorhamnetin	C16H12O7	316.058	316.0583	-1.1	+H	299.0550; 163.0754; 271.0601
5	4.63	4',5,7-trihydroxy-6-methoxyisoflavone 7-o-β-d-xylopyranosyl-(1→6)-β-d-glucopyranoside	C27H30O15	594.1591	594.15847	1	+H, +K, +Na	579.1708; 313.0707; 415.1024
6	4.78	Daidzein-4,7-diglucoside	C27H30O14	578.1644	578.16356	1.5	+H, +K, +Na	297.0758; 399.1074; 417.1180
7	5.04	4H-Benzopyran-4-one, 6-beta-D-glucopyranosyl-5-hydroxy-2-(4-hydroxyphenyl)-7-methoxy-	C22H22O10	446.1207	446.1213	-1.4	+H	429.1180; 327.0863; 411.1074
8	5.27	Puerarin	C21H20O9	416.1108	416.11073	0.2	+H	255.0650; 237.0546; 279.0652
9	5.74	Isoschaftoside	C26H28O14	564.1482	564.14791	0.5	+H, +Na	433.1136; 415.1020; 313.0704
10	6.21	Puerarin xyloside II	C26H28O13	548.1534	548.15299	0.8	+H	531.1497; 399.1074; 381.0966
11	6.34	Tilianine	C22H22O10	446.1214	446.1213	0.1	+H, +Na	417.1180; 399.1074; 297.0758
12	6.55	4',6,7-trihydroxyisoflavone-6-methylether-7-o-β-d-xylopyranosyl-(1→6)-β-d-glucopyranoside	C27H30O14	578.1643	578.16356	1.2	+H	447.1286; 429.1180; 327.0853
13	6.92	Daidzein	C15H10O4	254.0575	254.05791	-1.5	+H	137.0233; 237.0546; 145.0284
14	7.61	Chrysophanol	C15H10O4	254.0578	254.05791	-0.2	+H	237.0546; 225.0547; 134.0358
15	7.71	Liquiritigenin	C15H12O4	256.0733	256.07356	-1.2	+H	239.0703; 147.0441; 163.0390
16	8.12	7,8,4'-Trihydroxyisoflavone	C15H10O5	270.0524	270.05282	-1.5	+H	153.0182; 253.0495; 134.0362
17	8.38	8-methoxy-5-o-glucoside flavone	C22H22O9	430.1258	430.12638	-1.4	+H, +Na	317.0656; 301.0707; 297.0758
18	8.89	7,4'-Dihydroxyflavone	C15H10O5	270.0526	270.05282	-0.7	+H	255.0652; 181.0495; 147.0437
19	9.68	Formononetin	C16H12O4	268.0734	268.07356	-0.7	+H	253.0495; 237.0546; 137.0233
20	10.27	Anemarchalconyn	C15H10O3	238.0628	238.06299	-0.7	+H	147.0441; 119.0491; 123.0440
21	12.24	Timosaponin B III	C45H74O18	902.488	902.48752	0.6	+H, +K	741.4420; 579.3712; 417.3363
22	12.99	Glycyrrhisoflavanone	C21H20O6	368.1258	368.12599	-0.6	+H, +K	193.0495; 167.0339; 205.0859
23	13.15	Pinocembrin	C15H12O4	256.0732	256.07356	-1.5	+H	137.0233; 239.0703; 151.0390
24	13.97	Timosaponin A3	C39H64O13	740.4346	740.43469	-0.2	+H	469.3312; 579.3892; 487.3418
25	14.36	Anhydroicaritin	C21H20O6	368.1254	368.12599	-1.6	+H, +Na	281.0441; 243.0652; 301.0707
26	14.68	Aurantiamid	C25H26N2O3	402.1937	402.19434	-1.6	+H, +K	385.1910; 119.0855
27	17.14	Licochalcone A	C21H22O4	338.1511	338.15181	-2	+H	297.1485; 229.0859; 271.0965
28	17.42	Timosaponin A-1	C33H54O8	578.3825	578.38187	1.2	+H	417.3363; 255.2107; 435.2745
29	17.51	Glycyrol	C21H18O6	366.1108	366.11034	1.3	+H	296.0315; 268.0366; 309.0394

regulated (Fig. 7A). Besides, levels of lipid oxidation and ROS detection with flow detection technology in MLE-12 cells demonstrated that TGF-β treatment could apparently elevate the levels of lipid oxidation and ROS in MLE-12 cells, which could be reduced to normal level after QF-containing serum treatment. Similarly, Erastin reversed the effect of QF and aggravate ROS and lipid oxidation in TGF-β-exposed MLE-12 cells (Fig. 7B,D). Additionally, Fe^{2+} level of the MLE-12 cells in the TGF-β treatment group was significantly elevated. The Fe^{2+} level in the TGF-β+QF serum treatment group was significantly decreased, while Erastin administration

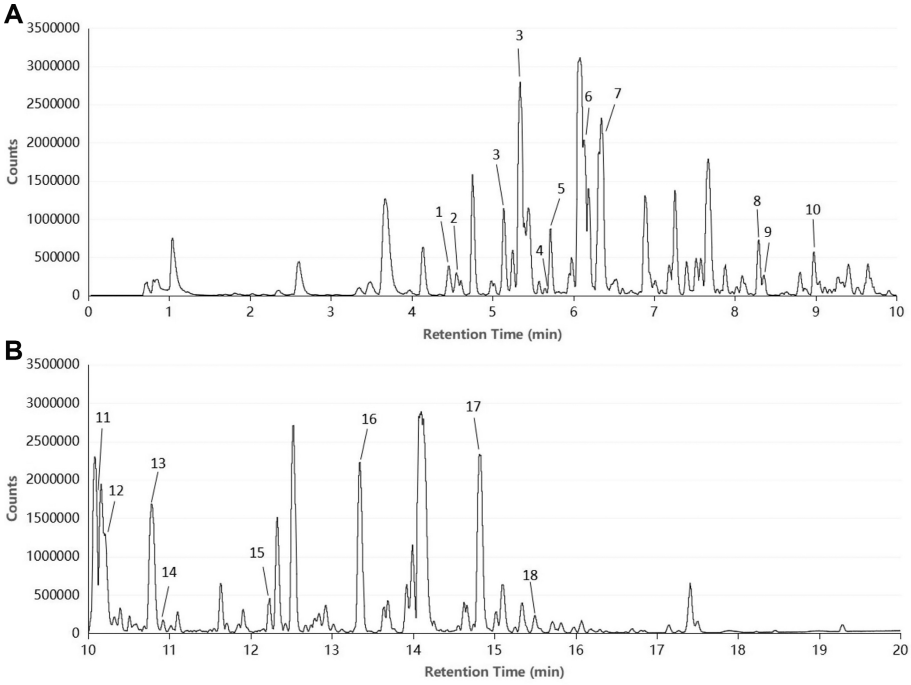

Fig. 3. BPI of extract under the negative ion mode. BPI of extract under the negative ion mode for 0-20 min. **A.** 0-10 min. **B.** 10-20 min.

Table 2. Identification of chemical constituents from extract (screening in the negative ion model).

No	Observation retention time (tR) (min)	Identification	Element composition	Observed molecular mass (Da)	Molecular mass(Da)	Error (ppm)	Adduct	Fragment ions
1	4.51	Scopoletol	C10H8O4	192.0424	192.04226	0.8	-H, +HCOO	177.0193; 161.0244; 109.0295
2	4.64	Nicotiflorin	C27H30O15	594.1594	594.15847	1.5	-H	473.1089; 310.0483; 430.0906
3	5.17	Neomangiferin	C25H28O16	584.1383	584.13773	1	-H	565.1199; 493.0988; 331.0459
4	5.67	Robinin	C33H40O19	740.2158	740.21638	-0.8	-H	295.0612; 577.1563; 415.0671
5	5.74	Isoschaftoside	C26H28O14	564.1481	564.14791	0.3	-H	431.0993; 417.1192; 311.0561
6	6.21	Puerarin xyloside II	C26H28O13	548.1536	548.15299	1.1	-H	421.0776; 301.0354; 272.0326
7	6.35	3'-Methoxypuerarin	C22H22O10	446.1221	446.1213	1.7	-H	325.0718; 415.1035; 207.0663
8	8.32	Glycyroside	C27H30O13	562.169	562.16864	0.6	-H	429.1191; 309.0768; 281.0823
9	8.38	Isoononin	C22H22O9	430.1269	430.12638	1.1	-H	149.0608; 205.0870; 285.0405
10	8.99	Naringenin	C15H12O5	272.069	272.06847	2	-H	135.0452; 135.0088
11	10.19	(25s)-26-o-β-d-glucopyranosyl-22-hydroxy-5β-furostane-3β,26-diol 3-o-β-d-glucopy-ranosyl-(1→2)-o-β-d-galactopyranoside	C45H76O19	920.4975	920.49808	-0.6	-H, +HCOO	757.4380; 595.3852; 839.4071
12	10.34	Phebalosin	C15H14O4	258.0892	258.08921	-0.2	-H	227.0350; 135.0452
13	10.87	Licorice glycoside E	C35H35NO14	693.2062	693.20575	0.7	-H	549.1614; 531.1508; 473.1453
14	10.93	TimosaponinD	C45H74O19	918.4827	918.48243	0.3	-H, +HCOO	755.4223; 611.3801; 657.3856
15	12.34	Xilingsaponin B	C45H74O18	902.4893	902.48752	1.9	+HCOO, -H	739.4274; 821.3965; 577.3746
16	13.29	Licoricesaponin E2	C42H60O16	820.388	820.38814	-0.2	-H	351.0569; 517.3171; 775.3910
17	14.82	Glyeurysaponin	C42H62O16	822.4041	822.40379	0.4	-H	703.3699; 661.3593; 645.3644
18	15.51	Anemarrhenasapinin III	C39H64O14	756.4305	756.42961	1.2	+HCOO, -H	593.3695; 501.3222; 467.2818

impaired the role of QF-containing serum in MLE-12 cells (Fig. 7C,E,F). The results of cell subcellular structure showed that the mitochondrial shape and size of cells became smaller after TGF-β treatment and mitochondrial ridges decreased. However, the mitochondrial damage was alleviated by QF-containing serum treatment, which was further aggravated after the addition of the ferroptosis inducer Erastin (Fig. 7G). It suggested that QF-containing serum inhibited cell viability, lipid oxidation level, ROS level, Fe^{2+} level and mitochondrial damage of MLE-12 cells induced by TGF-β by inhibiting ferroptosis.

Table 3. The time-course observation of mortality of mice treated with QF and Erastin.

Week	Group								Mortality
	1	2	3	4	5	6	7	8	(number of deaths/total)
Control	0	0	0	0	0	0	0	0	0/20 (0%)
IPF	3	2	2	1	0	0	2	1	11/20 (55%)
IPF+QF	2	1	1	0	0	0	0	0	4/20 (20%)
IPF+QF++Erastin	2	2	2	0	1	1	0	0	8/20 (40%)

From the beginning of treatment to another month after the end of treatment, observe the time ponits and the death of mice.

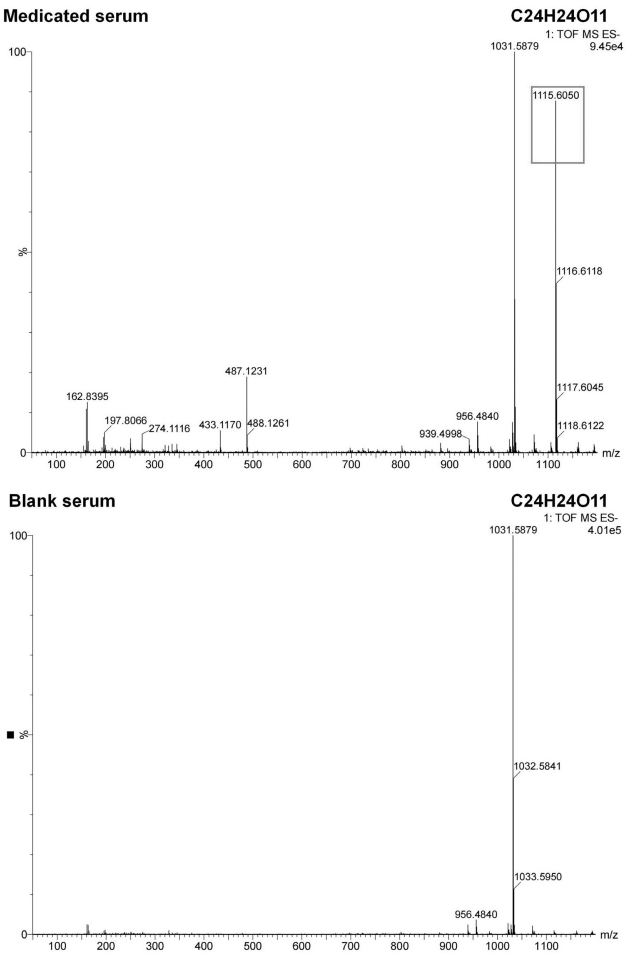

Fig. 4. Mass spectrum chromatograms of ingredients in the drug-containing serum and blank serum.

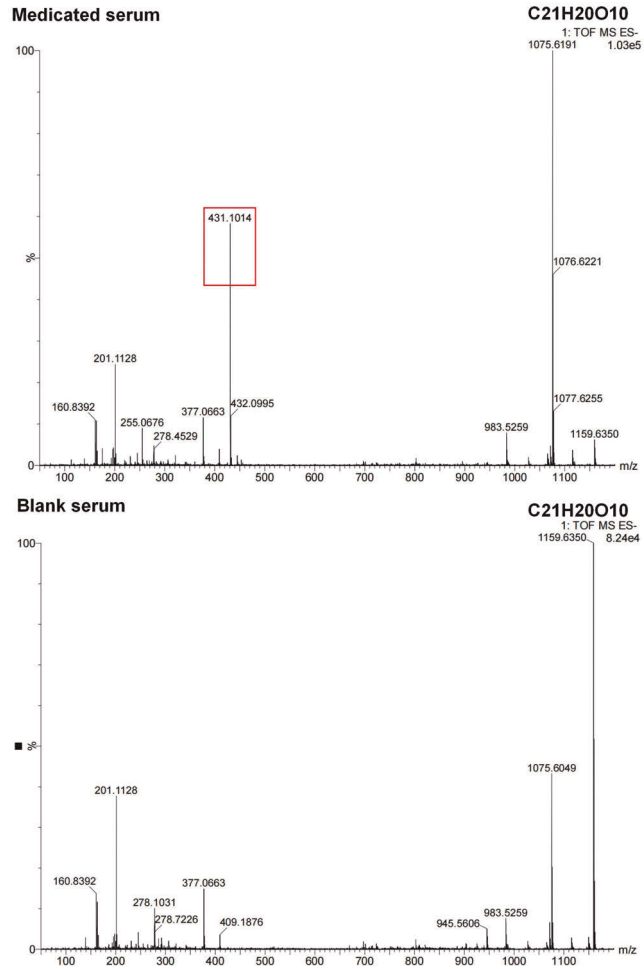

Fig. 5. Mass spectrum chromatograms of ingredients in the drug-containing serum and blank serum.

QF inhibits ferroptosis to alleviate the process of TGF-β-induced fibrosis by regulating the ACE2-ERK signaling pathway

Although QF blocked TGF-β-induced fibrosis in MLE-12 cells by inhibiting ferroptosis, the underlying mechanism remained unclear. It was observed that protein levels of ACE2 declined and phosphorylated ERK was elevated in the presence of TGF-β, which were reversed by QF-containing serum treatment. However, Erastin exposure abolished the role of QF-containing serum in TGF-β-challenged MLE-12 cells (Fig. 8A). Additionally, TGF-β also reduced the protein levels of FTH1 and Gpx4 in MLE-12 cells, while it promoted protein expressions of COX-2, ACSL4 and NOX1 protein levels. Both of them were reversed by QF-containing serum administration. After adding the ferroptosis inducer Erastin, the levels of FTH1, and Gpx4 proteins were significantly decreased, and COX-2, ACSL4 and NOX1 proteins were significantly increased (Fig. 8B). It was indicated that QF-containing serum possibly alleviates the process of fibrosis through inhibiting ferroptosis by regulating ACE2-ERK pathway.

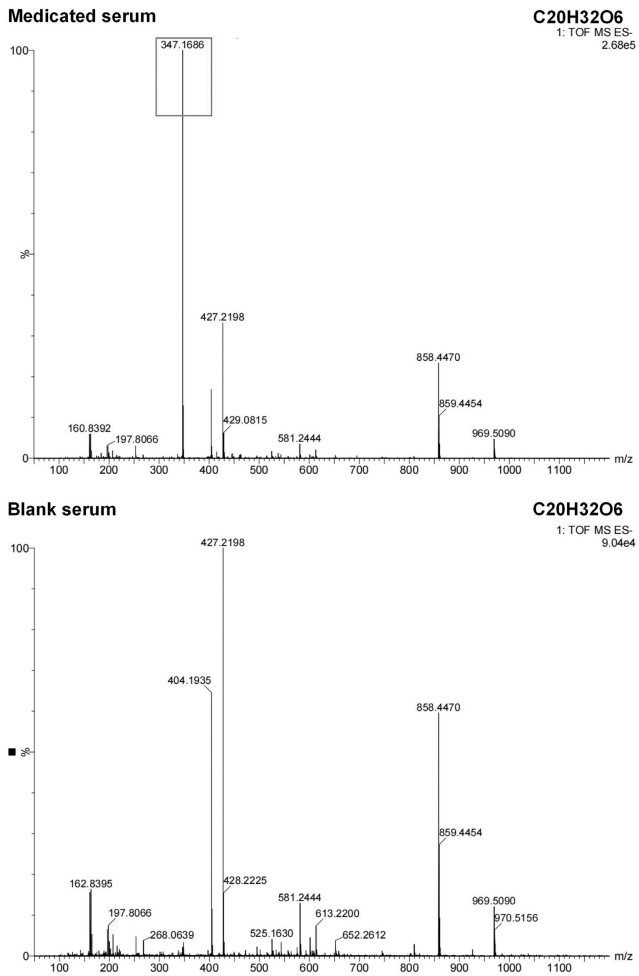

Fig. 6. Mass spectrum chromatograms of ingredients in the drug-containing serum and blank serum.

QF relieves the secretion of inflammatory factors in IPF mice through inhibiting ferroptosis

The roles of QF on the process of lung fibrosis in mice were investigated in a bleomycin-induced IPF animal model *in vivo*. The mortality rate of mice in the IPF group was significantly increased, which was notably relieved in QF-treated group. However, the mice injected with the iron death inducer Erastin were found with an elevated mortality rate (Fig. 9A, Table 3). Subsequently, the lungs and body weights of the mice were weighed. The results showed the lung coefficient of the mice in the IPF group was significantly increased, and the body weight and lung dry weight were significantly decreased compared with the control group. QF administration relieved the pulmonary fibrosis progression with the reduction of pulmonary index and lung dry weight, whereas Erastin abrogated the effects of QF in IPF mice (Fig. 9B). Additionally, serum inflammation-related factors in mice were detected with ELISA. Compared with the control group, the serum TGF-β1, IL-6 and IL-17 contents of the mice in the IPF group were significantly increased, which were downregulated in the QF treatment group and elevated in the Erastin group (Fig. 9C). Therefore, QF significantly inhibited the lung coefficient, lung dry weight and inflammation-related factors in IPF mice through regulating ferroptosis.

QF alleviates pathological degree of pulmonary fibrosis in bleomycin-induced mice

Subsequently, HE, Masson and IHC staining were conducted to detect the degree of fibrosis in the mouse lung tissue. The results showed that the lung structure of the control group was clear without inflammation, inflammatory cell infiltration and fibrosis. In the IPF group, the alveolar septum of the lung tissue was significantly widened, and the alveolar cavity was narrow, accompanied with inflammatory cell infiltration, which reflected in macrophages and activated fibroblasts, and sheet-like hyperplasia collagen fibers in the alveolar septum and inflammatory area, indicating the high degree of fibrosis (Fig. 10A,D). Masson staining proved that fibrils of different sizes were aggregated in the form of filaments or bundles, and the collagen around blood vessels and bronchioles was obviously widened (Fig. 10B,E), and the expression of Collagen I protein in cells was significantly increased. However, pulmonary fibrosis in the QF treatment group was gradually alleviated, and the Collagen I protein was significantly reduced. Erastin further deepened the lung tissue fibrosis and increased Collagen I protein level (Fig. 10C,F). It is demonstrated that QF effectively inhibits the degree of pulmonary fibrosis in bleomycin-induced mice.

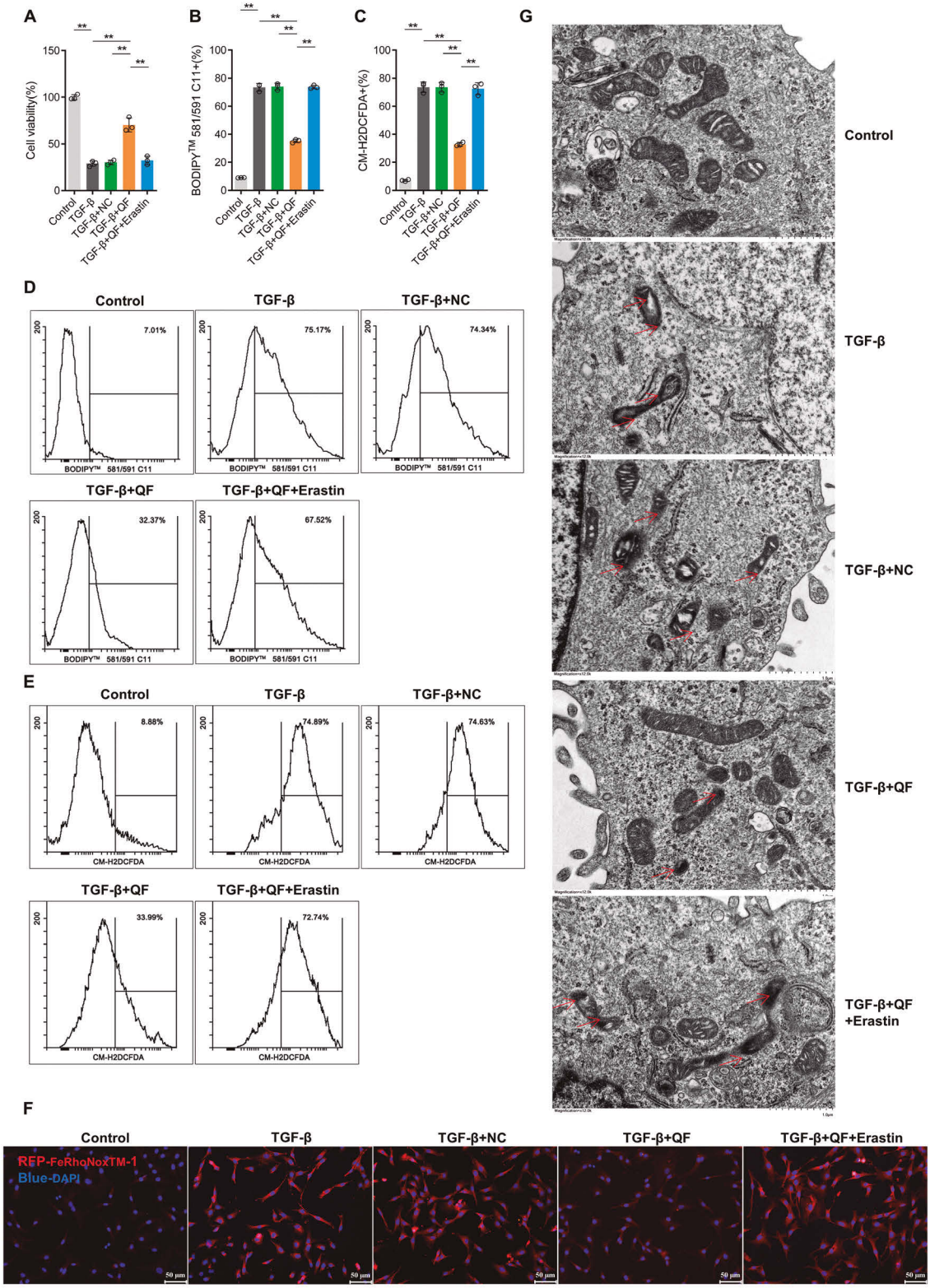

Fig. 7. QF-containing serum attenuated TGF-β-induced fibrosis in MLE-12 cells by blocking ferroptosis. **A.** Cell activities of each group were detected by CCK8. **B, D.** Intracellular lipid oxidation level was detected with BODIPYTM 581/591 C11 lipid oxidation probe. **C, E.** Intracellular total ROS level was detected with CM-H2DCFDA probe. **F.** Intracellular Fe2+ level was determined with FeRhoNoxTM-1 fluorescent probe. **G.** Cell substructure was observed with TEM. NC: negative control group, TGF-β: TGF-β induced group, TGF-β+NC: TGF-β induced group and treated with negative control DMSO, TGF-β+QF: TGF-β induced group and treated with QF, TGF-β+QF+Erastin: TGF-β induced group and treated with QF and Erastin. Data are shown as the mean ± SD, n=3, *p<0.05 and **p<0.01.

QF relieves pathological degree of pulmonary fibrosis in bleomycin-induced mice possibly by activating ACE2-ERK pathway

The *in vitro* results had proved that QF could block ferroptosis via regulating the ACE2-ERK pathway to inhibit the degree of cell fibrosis. Whether QF could alter ACE2-ERK pathway to regulate ferroptosis in the process of mouse fibrosis *in vivo* remained unclear. The results showed that the levels of MDA, ROS and Fe^{2+} in the lung tissue of the bleomycin-induced mice were significantly increased compared to the control group.

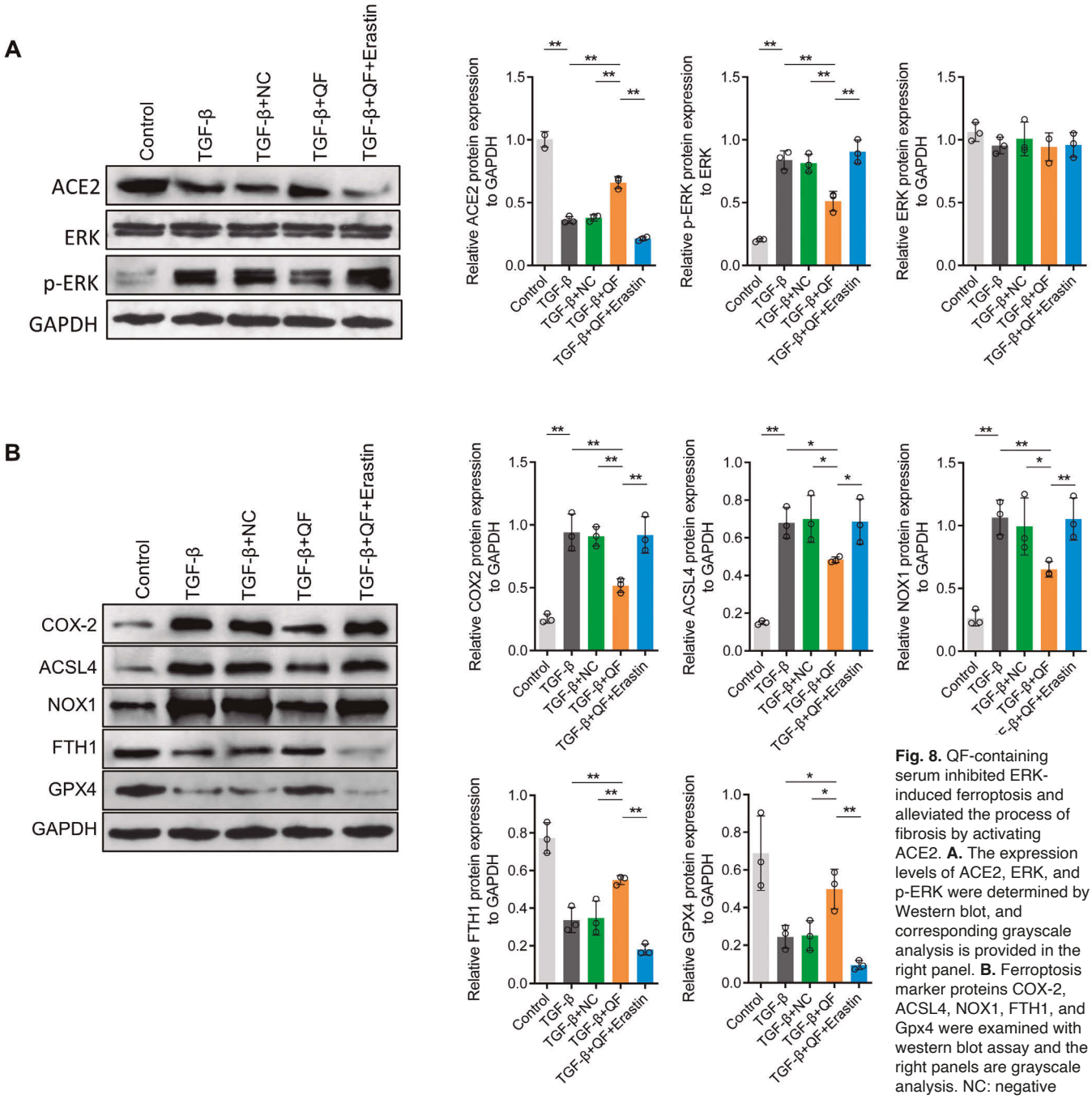

Fig. 8. QF-containing serum inhibited ERK-induced ferroptosis and alleviated the process of fibrosis by activating ACE2. **A.** The expression levels of ACE2, ERK, and p-ERK were determined by Western blot, and corresponding grayscale analysis is provided in the right panel. **B.** Ferroptosis marker proteins COX-2, ACSL4, NOX1, FTH1, and Gpx4 were examined with western blot assay and the right panels are grayscale analysis. NC: negative control group, TGF-β: TGF-β induced group, TGF-β+NC: TGF-β induced group and treated with negative control DMSO, TGF-β+QF: TGF-β induced group and treated with QF, TGF-β+QF+Erastin: TGF-β induced group and treated with QF and Erastin. Data are shown as the mean ± SD. *p<0.05 and **p<0.01.

QF treatment significantly reduced the levels of MDA, ROS and Fe^{2+}, while the ferroptosis inducer Erastin treatment notably upregulated the levels of MDA, ROS and Fe^{2+} in IPF mice (Fig. 11A-C). Besides, in bleomycin-induced mice model, the protein levels of ACE2, FTH1, and Gpx4 in the lung tissue were significantly decreased, and the phosphorylation level of ERK, COX-2, ACSL4, and NOX1 protein levels were significantly increased, which was consistent with the results in TGF-β induced MLE-12 cells. Similarly, QF could effectively relieve the changes of ACE2-ERK pathway and its-related signaling molecules, while Erastin abolished the protective role of QF in IPF mice (Fig. 11D-E). Thus, QF might alleviate the process of IPF by activating ACE2 and inhibiting ERK-induced ferroptosis *in vivo*.

Discussion

IPF is a chronic, debilitating and often fatal lung disease, and numerous studies have investigated the potential efficacy and benefits of herbal medicines for IPF in the past few years (Yao and Jiang, 2003; Li and Kan, 2017). In the present study, it was found that QF

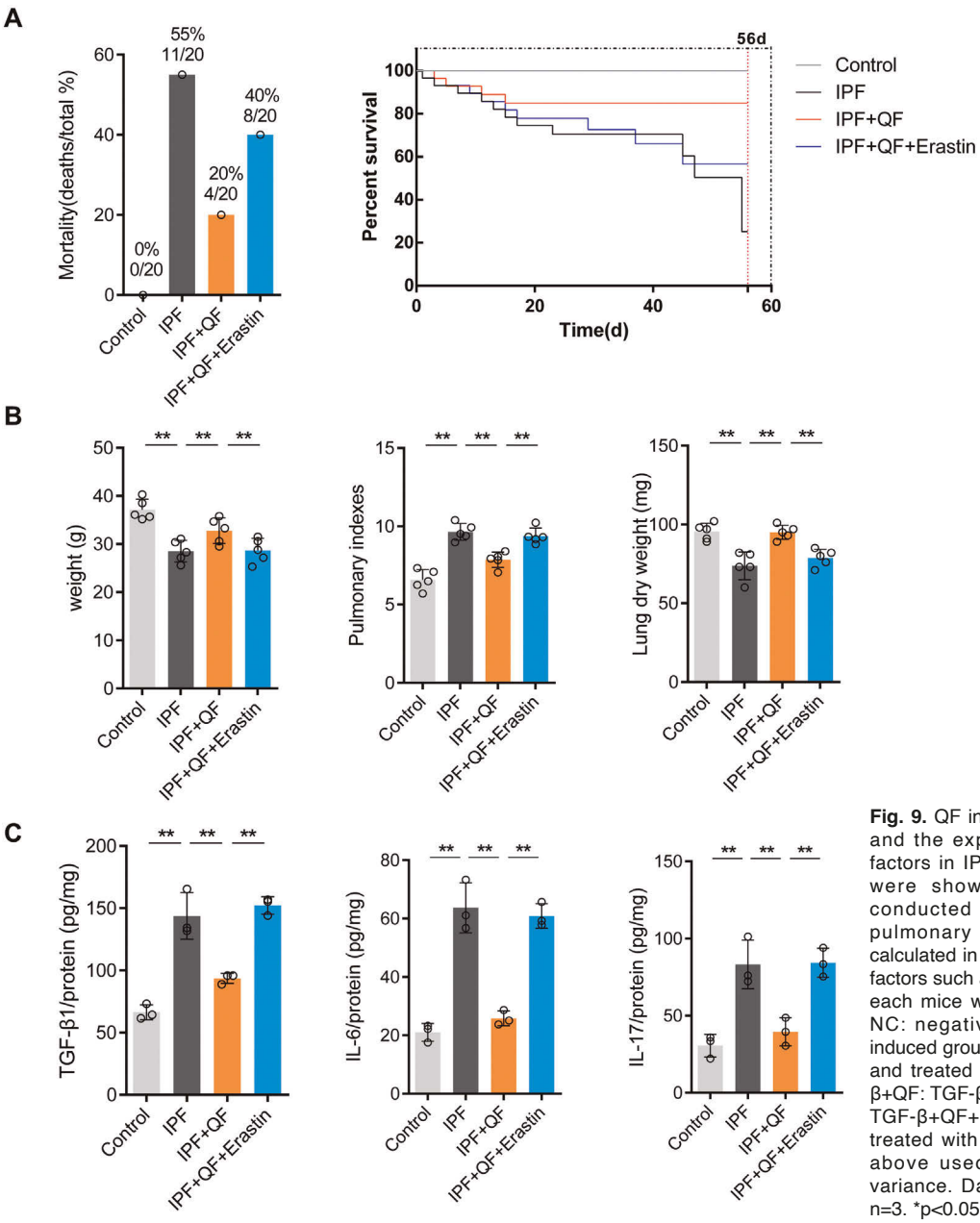

Fig. 9. QF inhibited lung coefficient, body weight and the expression of inflammation-related factors in IPF mice. **A.** Mice survival statistics were shown and survival analysis were conducted in each group. **B.** Mice weight, pulmonary index and lung dry weight were calculated in each group. **C.** Inflammation-related factors such as TGF-β, IL-6 and IL-17 in serum of each mice were determined with ELISA assay. NC: negative control group, TGF-β: TGF-β induced group, TGF-β+NC: TGF-β induced group and treated with negative control DMSO, TGF-β+QF: TGF-β induced group and treated with QF, TGF-β+QF+Erastin: TGF-β induced group and treated with QF and Erastin. All data analysis above used One-Way ANOVA analysis of variance. Data are shown as the mean ± SD, n=3. *p<0.05 and **p<0.01.

could alleviate the process of IPF by activating ACE2 and inhibiting ferroptosis in TGF-β-induced MLE-12 cells and a bleomycin-induced IPF mice model. The pathogenesis of pulmonary fibrosis is related to ferroptosis and mitochondrial dysfunction. Ferroptosis inhibitors have been reported to alleviate radiation-induced pulmonary fibrosis (RILF) by downregulating TGF-β1 (Li et al., 2019). Herein, we also proved that QF improved IPF possibly by inhibiting ferroptosis. These findings provide important references for traditional Chinese Medicine in the treatment of pulmonary fibrosis.

As a Chinese patent medicine, QF has a protective effect on pulmonary fibrosis caused by bleomycin. QF has been reported to reduce the degree of proliferation of fibroblasts and the consequent collagen content and

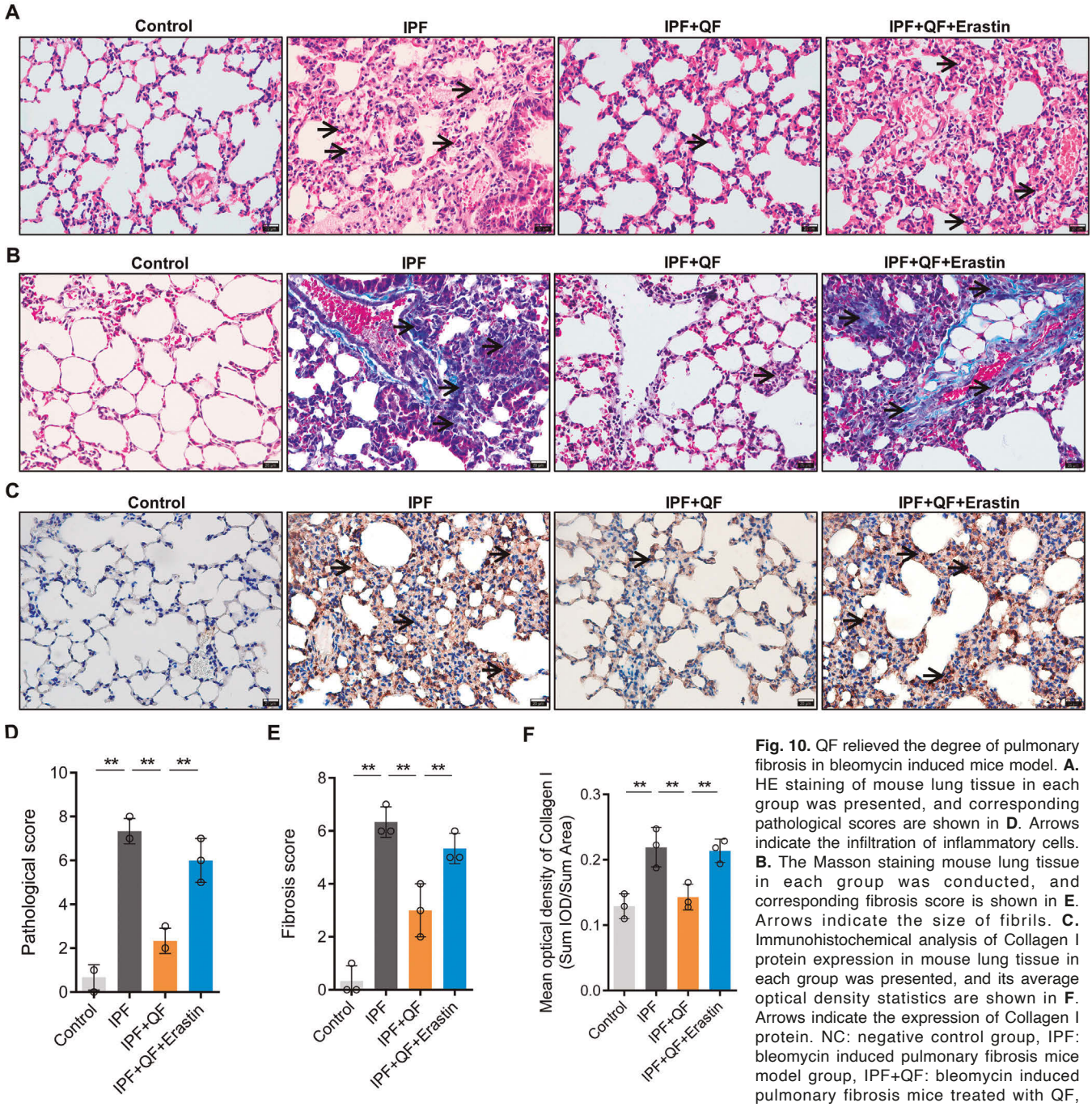

Fig. 10. QF relieved the degree of pulmonary fibrosis in bleomycin induced mice model. **A.** HE staining of mouse lung tissue in each group was presented, and corresponding pathological scores are shown in **D**. Arrows indicate the infiltration of inflammatory cells. **B.** The Masson staining mouse lung tissue in each group was conducted, and corresponding fibrosis score is shown in **E**. Arrows indicate the size of fibrils. **C.** Immunohistochemical analysis of Collagen I protein expression in mouse lung tissue in each group was presented, and its average optical density statistics are shown in **F**. Arrows indicate the expression of Collagen I protein. NC: negative control group, IPF: bleomycin induced pulmonary fibrosis mice model group, IPF+QF: bleomycin induced pulmonary fibrosis mice treated with QF, IPF+QF+Erastin: bleomycin induced pulmonary fibrosis mice treated with QF and Erastin. All data analysis above used One-Way ANOVA analysis of variance. Data are shown as the mean ± SD, n=3. *p<0.05 and **p<0.01.

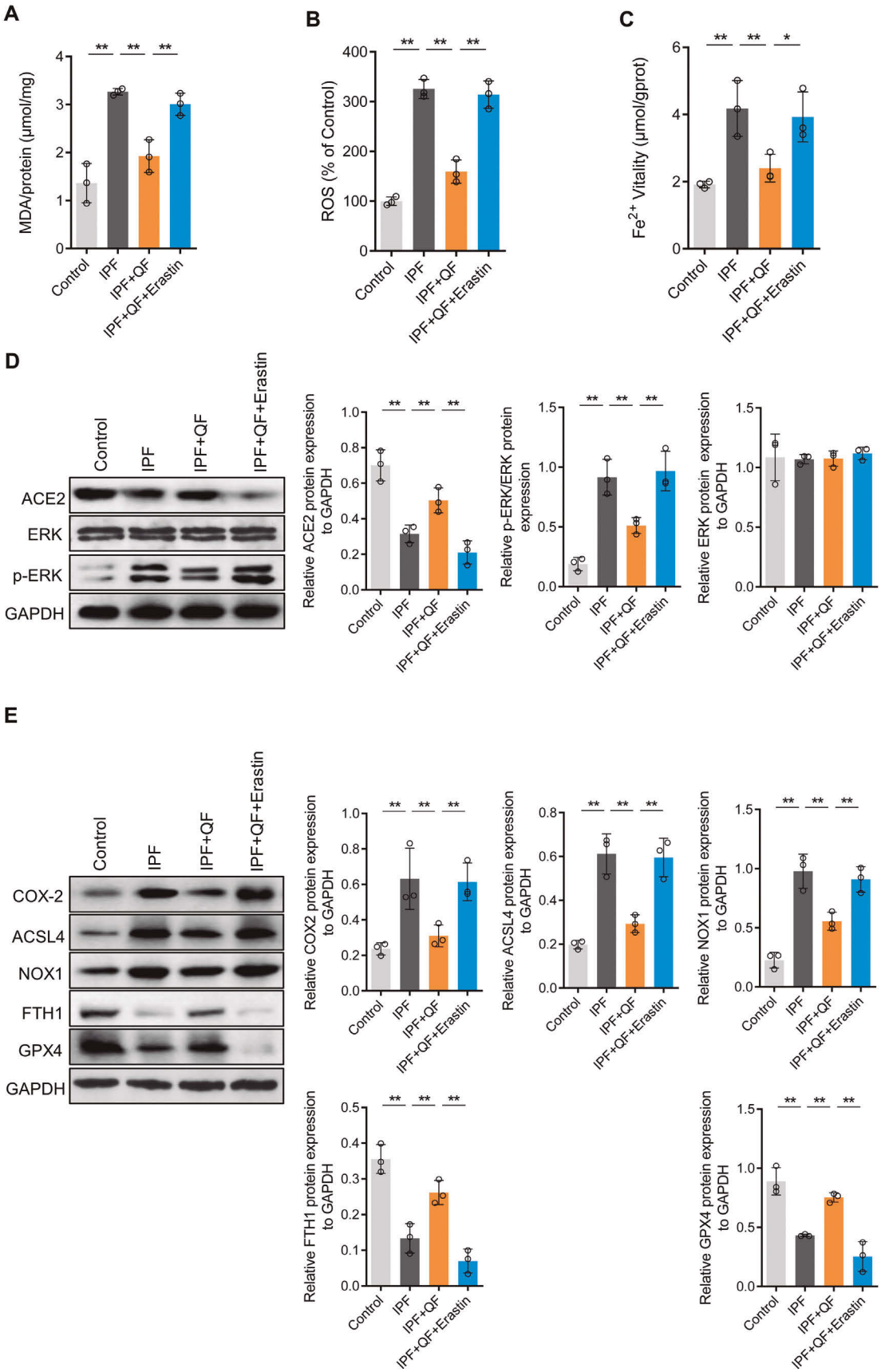

Fig. 11. QF alleviated pulmonary fibrosis by activating ACE2 and blocking ERK-induced ferroptosis in bleomycin induced mice model. **A-C.** MDA, ROS and Fe2+ level in mice lung tissue of each group were calculated. **D.** The expression levels of ACE2, ERK, and p-ERK from lung tissues in mice were determined by Western blot, and corresponding grayscale analysis is provided in the right panel. **E.** Ferroptosis marker proteins COX-2, ACSL4, NOX1, FTH1, and Gpx4 were examined with western blot assay, and the right panels are the respective grayscale analyses. NC: negative control group, IPF: bleomycin induced pulmonary fibrosis mice model group, IPF+QF: bleomycin induced pulmonary fibrosis mice treated with QF, IPF+QF+Erastin: bleomycin induced pulmonary fibrosis mice treated with QF and Erastin. All data analysis above used One-Way ANOVA analysis of variance. Data are shown as the mean ± SD, n=3. *p<0.05 and **p<0.01.

improve the development of pathological fibrosis in the lung, indicating that QF has anti-fibrotic effects and may be helpful in treating pulmonary fibrosis (Sun et al., 2018). Our results showed that TGF-β induced the increase of a-SMA, Collagen I and reduced cell viability in MLE-12 cells. QF-containing serum administration promoted the cell viability in the process of pulmonary fibrosis, indicating that QF-containing serum had anti-fibrotic activity. Traditional Chinese herbal extracts Tanshinone IIA (TIIA) and osthole have been reported to alleviate bleomycin-induced pulmonary fibrosis *in vitro* and *in vivo*, possibly by modulating the ACE-2/ANG-(1-7) axis to reduce inflammation (Wu et al., 2014; Hao and Liu, 2016). Recently, Traditional Chinese Medicine has been reported to have an improving effect on Covid-19, which is accompanied by the clinical manifestations of pulmonary fibrosis (Li et al., 2020). It is speculated that the potential therapeutic effect of Traditional Chinese Medicine is to directly inhibit the adsorption of the virus to host cells and its replication by binding to ACE2 receptors and 3C-like protease. Our results indicated that QF could reverse TGF-β-induced ACE2 reduction in MLE-12 cell and mouse model of pulmonary fibrosis. The Ace agonist xanthone has been reported to significantly reduce tacrolimus-induced elevation of renal p-ERK1/2 expression to normal levels (Azouz et al., 2022). Our results also confirmed that QF downregulated p-ERK levels in TGF-β-induced fibrosis and bleomycin-induced mouse PF model. These results suggested that QF might reactivate ACE2 activity by inhibiting the p-ERK/ERK pathway. QF-mediated reactivation of ACE2 may be one of the main pathways to improve IPF.

Ferroptosis mediates the occurrence and development of pulmonary diseases, and regulation of ferroptosis may be a promising strategy for clinical treatment of pulmonary diseases (Ma et al., 2021). Tongxinluo, a Traditional Chinese Medicine, protects pulmonary microvascular barrier dysfunction by inhibiting ferroptosis and prevents chronic obstructive pulmonary disease (Wang et al., 2022). Our results showed that QF could alleviate the phenomenon of ferroptosis in TGF-β-induced fibrosis, and Erastin could block the therapeutic effect of QF in fibrosis models *in vitro* and *in vivo*, and aggravate the damage of lung tissue. The results showed that the improvement of IPF by QF depended on the ferroptosis signal. The renin-angiotensin system is implicated in the pathogenesis of pulmonary hypertension and pulmonary fibrosis, both of which are common in chronic lung diseases such as chronic obstructive pulmonary disease (Kuba et al., 2006). Ferrostatin-1, a ferroptosis inhibitor, alleviates Ang II-mediated cardiac fibrosis in mice (Zhang et al., 2022). This evidence indicates that ferroptosis is involved in fibrotic disease progression via the ACE2-renin-angiotensin system. In our study, we demonstrated that QF improved IPF, accompanied by the inhibition in ferroptosis and the reactivation of ACE2. Therefore, QF alleviated IPF possibly by regulating renin-angiotensin, and subsequently blocking ferroptosis by affecting ACE2-ERK signaling axis.

Although our results confirmed that QF had anti-fibrotic effects *in vitro* and *in vivo*, and elucidate the regulation mechanism, there were other issues that needed to be further elucidated. Firstly, we did not clearly point out that QF inhibited ferroptosis by activating ACE2, which needs to be confirmed in combination with intracellular ACE2 gain and loss. Next, whether QF altered ACE2 activity via the ERK pathway remained unclear, which should be verified in combination with ERK pathway agonist. Finally, this study lacked the support of clinical data.

In conclusion, the results confirmed that QF alleviated IPF by regulating renin-angiotensin and blocking ferroptosis. In summary, this research clarified the mechanism of QF mediated anti-IPF effect and provided a meaningful strategy for IPF treatment.

Ethics approval and consent to participate. All animal experiments were approved by Zhejiang Center of Laboratory Animals (Animal ethics No. ZJCLA-IACUC-20050061).

Funding. This work was supported by Zhejiang Provincial Natural Science Foundation of China under Grant No.LY21H010001; Zhejiang Provincial Traditional Chinese Medicine Science and Technology Project under Grant No.2021ZB219.

Competing interests. All authors declare no competing interests.

References

Azouz A.A., Omar H.A., Hersi F., Ali F.E.M. and Hussein Elkelawy A.M.M. (2022). Impact of the ACE2 activator xanthenone on tacrolimus nephrotoxicity: Modulation of uric acid/ERK/p38 MAPK and Nrf2/SOD3/GCLC signaling pathways. Life Sci. 288, 120154.

Bringardner B.D., Baran C.P., Eubank T.D. and Marsh C.B. (2008). The role of inflammation in the pathogenesis of idiopathic pulmonary fibrosis. Antioxid. Redox Signal. 10, 287-301.

Chu H., Shi Y., Jiang S., Zhong Q., Zhao Y., Liu Q., Ma Y., Shi X., Ding W., Zhou X., Cui J., Jin L., Guo G. and Wang J. (2017). Treatment effects of the traditional chinese medicine shenks in bleomycin-induced lung fibrosis through regulation of TGF-beta/Smad3 signaling and oxidative stress. Sci. Rep. 7, 2252.

Dixon S.J., Lemberg K.M., Lamprecht M.R., Skouta R., Zaitsev E.M., Gleason C.E., Patel D.N., Bauer A.J., Cantley A.M., Yang W.S., Morrison B. 3rd and Stockwell B.R. (2012). Ferroptosis: An iron-dependent form of nonapoptotic cell death. Cell 149, 1060-1072.

Fraser E. and Hoyles R.K. (2016). Therapeutic advances in idiopathic pulmonary fibrosis. Clin. Med. 16, 42-51.

George G., Vaid U. and Summer R. (2016). Therapeutic advances in idiopathic pulmonary fibrosis. Clin. Pharmacol. Ther. 99, 30-32.

Gong Y., Wang N., Liu N. and Dong H. (2019). Lipid peroxidation and GPX4 inhibition are common causes for myofibroblast differentiation and ferroptosis. DNA Cell Biol. 38, 725-733.

Hao Y. and Liu Y. (2016). Osthole alleviates bleomycin-induced pulmonary fibrosis via modulating angiotensin-converting enzyme 2/angiotensin-(1-7) axis and decreasing inflammation responses in rats. Biol. Pharm. Bull. 39, 457-465.

Harari S., Caminati A., Madotto F., Conti S. and Cesana G. (2017). Epidemiology, survival, incidence and prevalence of idiopathic pulmonary fibrosis in the USA and canada. Eur. Respir. J. 49, 1601504.

Kuba K., Imai Y. and Penninger J.M. (2006). Angiotensin-converting enzyme 2 in lung diseases. Curr. Opin. Pharmacol. 6, 271-276.

Kumar M., Prasad S.K. and Hemalatha S. (2014). A current update on the phytopharmacological aspects of *Houttuynia cordata* Thunb. Pharmacogn Rev. 8, 22-35.

Ley B. and Collard H.R. (2013). Epidemiology of idiopathic pulmonary fibrosis. Clin. Epidemiol. 5, 483-492.

Li L.C. and Kan L.D. (2017). Traditional Chinese medicine for pulmonary fibrosis therapy: Progress and future prospects. J. Ethnopharmacol. 198, 45-63.

Li X., Duan L., Yuan S., Zhuang X., Qiao T. and He J. (2019). Ferroptosis inhibitor alleviates radiation-induced lung fibrosis (RILF) via down-regulation of TGF-β1. J. Inflamm. 16, 11.

Li J., Cao F., Yin H.L., Huang Z.J., Lin Z.T., Mao N., Sun B. and Wang G. (2020). Ferroptosis: Past, present and future. Cell Death Dis. 11, 88.

Li S., Zhou C., Zhu Y., Chao Z., Sheng Z., Zhang Y. and Zhao Y. (2021). Ferrostatin-1 alleviates angiotensin II (Ang II)- induced inflammation and ferroptosis in astrocytes. Int. Immunopharmacol. 90, 107179.

Ma T.L., Zhou Y., Wang C., Wang L., Chen J.X., Yang H.H., Zhang C.Y., Zhou Y. and Guan C.X. (2021). Targeting ferroptosis for lung diseases: Exploring novel strategies in ferroptosis-associated mechanisms. Oxid. Med. Cell. Longev. 2021, 1098970.

Meyer K.C. (2017). Pulmonary fibrosis, part I: Epidemiology, pathogenesis, and diagnosis. Expert Rev. Respir. Med. 11, 343-359.

Molteni A., Wolfe L.F., Ward W.F., Ts'ao C.H., Molteni L.B., Veno P., Fish B.L., Taylor J.M., Quintanilla N., Herndon B. and Moulder J.E. (2007). Effect of an angiotensin II receptor blocker and two angiotensin converting enzyme inhibitors on transforming growth factor-beta (TGF-beta) and alpha-actomyosin (alpha SMA), important mediators of radiation-induced pneumopathy and lung fibrosis. Curr. Pharm. Des. 13, 1307-1316.

Prata L.O., Rodrigues C.R., Martins J.M., Vasconcelos P.C., Oliveira F.M., Ferreira A.J., Rodrigues-Machado M.D. and Caliari M.V. (2017). Original research: ACE2 activator associated with physical exercise potentiates the reduction of pulmonary fibrosis. Exp. Biol. Med. 242, 8-21.

Rashidipour N., Karami-Mohajeri S., Mandegary A., Mohammadinejad R., Wong A., Mohit M., Salehi J., Ashrafizadeh M., Najafi A. and Abiri A. (2020). Where ferroptosis inhibitors and paraquat detoxification mechanisms intersect, exploring possible treatment strategies. Toxicology 433-434, 152407.

Shenoy V., Ferreira A.J., Qi Y., Fraga-Silva R.A., Diez-Freire C., Dooies A., Jun J.Y., Sriramula S., Mariappan N., Pourang D., Venugopal C.S., Francis J., Reudelhuber T., Santos R.A., Patel J.M., Raizada M.K. and Katovich M.J. (2010). The angiotensin-converting enzyme 2/angiogenesis-(1-7)/mas axis confers cardiopulmonary protection against lung fibrosis and pulmonary hypertension. Am. J. Respir. Crit. Care Med. 182, 1065-1072.

Shenoy V., Qi Y., Katovich M.J. and Raizada M.K. (2011). ACE2, a promising therapeutic target for pulmonary hypertension. Curr. Opin. Pharmacol. 11, 150-155.

Strongman H., Kausar I. and Maher T.M. (2018). Incidence, prevalence, and survival of patients with idiopathic pulmonary fibrosis in the UK. Adv. Ther. 35, 724-736.

Sun L., Mao M., Yan Z., Zuo C. and Zhang X. (2018). A chinese traditional therapy for bleomycin-induced pulmonary fibrosis in mice. Can. Respir J. 2018, 8491487.

Uhal B.D., Kim J.K., Li X. and Molina-Molina M. (2007). Angiotensin-TGF-beta 1 crosstalk in human idiopathic pulmonary fibrosis: Autocrine mechanisms in myofibroblasts and macrophages. Curr. Pharm. Des. 13, 1247-1256.

Uhal B.D., Li X., Piasecki C.C. and Molina-Molina M. (2012). Angiotensin signalling in pulmonary fibrosis. Int. J. Biochem. Cell Biol. 44, 465-468.

Wang R., Ibarra-Sunga O., Verlinski L., Pick R. and Uhal B.D. (2000). Abrogation of bleomycin-induced epithelial apoptosis and lung fibrosis by captopril or by a caspase inhibitor. Am. J. Physiol. Lung Cell Mol. Physiol. 279, L143-151.

Wang Y., Kuang X., Yin Y., Han N., Chang L., Wang H., Hou Y., Li H., Li Z., Liu Y., Hao Y., Wei Y., Wang X. and Jia Z. (2022). Tongxinluo prevents chronic obstructive pulmonary disease complicated with atherosclerosis by inhibiting ferroptosis and protecting against pulmonary microvascular barrier dysfunction. Biomed. Pharmacother. 145, 112367.

Wu H., Li Y., Wang Y., Xu D., Li C., Liu M., Sun X. and Li Z. (2014). Tanshinone IIA attenuates bleomycin-induced pulmonary fibrosis via modulating angiotensin-converting enzyme 2/ angiotensin-(1-7) axis in rats. Int. J. Med. Sci. 11, 578-586.

Xu W., Deng H., Hu S., Zhang Y., Zheng L., Liu M., Chen Y., Wei J., Yang H. and Lv X. (2021). Role of ferroptosis in lung diseases. J. Inflamm. Res. 14, 2079-2090.

Yao C.F. and Jiang S.L. (2003). Prevention and treatment of pulmonary-fibrosis by traditional chinese medicine. Zhong Xi Yi Jie He Xue Bao. 1, 234-238 (in Chinese).

Yuan Q.J., Zhang Z.Y., Hu J., Guo L.P., Shao A.J. and Huang L.Q. (2010). Impacts of recent cultivation on genetic diversity pattern of a medicinal plant, *Scutellaria baicalensis* (Lamiaceae). BMC Genet. 11, 29.

Zhang X., Zheng C., Gao Z., Chen H., Li K., Wang L., Zheng Y., Li C., Zhang H., Gong M., Zhang H. and Meng Y. (2022). SLC7A11/xCT prevents cardiac hypertrophy by inhibiting ferroptosis. Cardiovasc. Drugs Ther. 36, 437-447.

Accepted April 11, 2024